# ac susceptibility and NMR observation of a deuterium isotope effect in the magnetization dynamics of the $Mn_{12}$-acetate nanomagnet

R. Blinc, B. Zalar, A. Gregorovič, D. Arčon, Z. Kutnjak, C. Filipič, and A. Levstik
*J. Stefan Institute, Jamova 39, 1000 Ljubljana, Slovenia*

R. M. Achey and N. S. Dalal
*Department of Chemistry and National High Magnetic Field Laboratory, Florida State University, Tallahassee, Florida 32306-4390*

(Received 15 July 2002; revised manuscript received 14 October 2002; published 6 March 2003)

The magnetization reversal dynamics of normal and deuterated $Mn_{12}$-acetate nanomagnets has been studied above the blocking temperature $T_B = 2.7$ K by ac magnetic susceptibility measurements between 100 Hz and 1 MHz and deuteron NMR relaxation. A pronounced isotope effect has been found which can be attributed to the changes in the strength of the hydrogen bonding of the water molecules on deuteration and the resulting changes in the spin-phonon coupling. Another point to be stressed is that the activation energy and relaxation rate obtained from our high-temperature–high-frequency magnetic susceptibility and deuteron NMR spin-lattice relaxation data are significantly higher than the one obtained from the low-temperature–low-frequency magnetization switching data.

DOI: 10.1103/PhysRevB.67.094401 PACS number(s): 76.60.−k, 75.50.Xx, 75.45.+j

## I. INTRODUCTION

Molecular clusters consisting of a large number of strongly coupled paramagnetic metal ions with a high spin ground state[1] offer the possibility to study the transition from molecular paramagnetism to bulk ferromagnetism. Of particular interest is the mechanism responsible for the reversal of the cluster magnetization.[2–4] Because of uniaxial anisotropy the $+m$ and $-m$ states are separated by a potential barrier, which may be overcome by thermally activated jumps over the potential barrier or by quantum resonant tunneling through the barrier.[1,4–7]

The best-studied example is the molecular magnet $[Mn_{12}O_{12}(CH_3COO)_{16}\cdot(H_2O)_4]\cdot 2CH_3COOH\cdot 4H_2O$, denoted as $Mn_{12}$-acetate.[1–7] The $Mn_{12}$ cluster consists of an outer ring of 8 $Mn^{3+}$ ions each with spin $S=2$ and an inner tetrahedron formed by 4 $Mn^{4+}$ ions each with a spin $S=\frac{3}{2}$. These two rings couple antiferromagnetically leading to a molecular total spin $S=10$ ground state. This spin state is in the tetragonal crystal field doubly degenerate in the absence of an external magnetic field. The magnetization switching between the two degenerate $m=\pm 10$ states has been so far studied by susceptibility and magnetization[1–6] as well as proton[8] and $^{55}$Mn NMR relaxation measurements.[9,10] It has been established that at low temperatures the magnetization reversal is exponential[1] following an initial short time recovery described by a square root of time $\sqrt{t}$ behavior.[11] The thermally activated type relaxation via phonon excitations has been described by

$$\tau = \tau_0 \exp\left[\frac{\Delta - g\mu_B \mathbf{S}\cdot\mathbf{B}}{kT}\right], \qquad (1)$$

where $\tau$ is the magnetization switching time, $\tau_0$ the inverse attempt frequency, the activation energy $\Delta$ represents the zero-field anisotropy induced barrier height for the ground state,[8–11] and $\mathbf{B}$ is the applied external magnetic field. Low-field–low-temperature susceptibility measurements show that the relaxation time for magnetization reversal in zero external magnetic field is indeed given by an Arrhenious law [Eq. (1)] with $\Delta/k = 64$ K and $\tau_0 = 2.6\times 10^{-7}$ s. The gradual decrease of the Arrhenius correlation time $\tau$ with increasing magnetic field $B$ is due to the reduction in the barrier height and is compatible with Eq. (1) for $S=10$ and $g=2$. The regular dips in the magnetic-field dependence of $\tau$ below 2 K,[8,9] on the other hand, are due to resonant quantum tunneling of the magnetization between different levels having the same energy in the two wells.

Proton spin-lattice relaxation time measurements,[6] which allow a direct determination of the correlation time $\tau = 1/\omega_L$ from the observed $T_1$ minimum at 60 K, yield, on the other hand, rather different $\tau$ values. These values are by two orders of magnitude faster than the ones extrapolated from the low-temperature susceptibility measurements and the above Arrhenius law. The reason for this discrepancy is still unknown and further checks are necessary. There is also a difference between the $\tau$ values deduced from $^{55}$Mn and $^{1}$H NMR data,[8,9] which has been interpreted as arising from the different time regimes of the two sets of measurements.

Recent electron paramagnetic resonance (EPR) measurements[12] suggest a possible breakdown of the total spin ($S=10$) description. A more microscopic approach based on $Mn^{3+}$-$Mn^{4+}$ pairs, has been proposed recently to explain the low-temperature $^{55}$Mn NMR relaxation and other data.[13] It should be also pointed out that proton,[14] deuteron,[15] and $^{13}$C NMR (Ref. 16) data show that the paramagnetic spin density of the cluster is at least in part delocalized over the entire molecule.

Here we report on ac susceptibility measurements on $Mn_{12}$-acetate and its deuterated analog at frequencies between 100 Hz and 1 MHz and temperatures between 4 and 20 K. The frequency range investigated is thus by three to four orders of magnitude larger than studied previously.[17] The larger frequency range allows for an analysis of the data using Cole-Cole plots. This approach yields a highly reliable

 

determination of the magnetization relaxation frequencies enabling us to search for possible deuteration isotope effects in the magnetization dynamics or a breakdown of the total spin $S=10$ description.

We also wished to check on the reported discrepancy[8] between the $\tau$ values obtained from proton NMR and low-frequency–low-temperature susceptibility measurements. We also decided to perform new deuteron spin-lattice relaxation time measurements at a different Larmor frequency than measured previously[15] and to compare the results with those obtained from proton NMR and susceptibility measurements. This should allow for a clear discrimination between Larmor frequency-dependent one-phonon spin-lattice relaxation processes and Larmor frequency-independent Raman-type processes recently suggested to be rate determining for the $^{55}$Mn relaxation.[13]

Another point to be investigated is the possible difference between the magnetization reversal behavior of $Mn_{12}$-acetate in the low-temperature and high-temperature regimes. Whereas it is conceivable that the total $S=10$ spin of the nanocluster is at least approximately a good quantum number at low temperatures this is not so obvious at high temperatures.

It should be noted that a recent neutron-diffraction[18] study showed that hydrogen bonding of the water molecules becomes stronger at temperatures below 20 K. For one-phonon processes the magnetization dynamics critically depends on the spin-phonon coupling and on the phonon velocity. In case of Raman processes it depends on the phonon frequencies. It is thus conceivable that in both cases changes in the hydrogen bonding strength with temperature[18] and deuteration affect the spin reversal dynamics.

The paper is organized as follows. Section II describes the theoretical models of ac susceptibility and deuteron spin-lattice relaxation in the total $S=10$ spin model. Section III contains the experimental details whereas the obtained results are analyzed and discussed in Sec. IV. The conclusions are summarized in Sec. V.

## II. THEORY

### A. ac spin susceptibility in the thermally activated regime

Let us first calculate the ac spin susceptibility in the thermally activated regime using the $S=10$ spin description. It should be noted that a similar calculation adapted for the low-temperature regime has been performed by J. Villain *et al.*[2] In their work only the leading transition terms have been kept resulting in an exponential relaxation rate. Here we want to extend this calculation to the high-temperature regime and therefore keep all the terms in the relaxation matrix.

The anisotropic potential acting on the cluster spin $S=10$ is dominated by the easy axis term[2,11]

$$\mathcal{H}_2^{(0)}=-\left(\frac{D}{S}\right)S_Z^2, \tag{2}$$

where $D\cong 6.1$ K. Only the two lowest energy levels $|10\rangle$ and $|-10\rangle$, coupled by a transverse field tunneling term, are important at low temperatures. At higher temperatures all ten doublets plus one singlet are involved. Let us now look into the linear response of this system when tunneling is neglected and a small ac magnetic field $\delta h$ is applied along the easy axis. The Hamiltonian now becomes

$$\mathcal{H}_2=-\left(\frac{D}{S}\right)S_Z^2-\gamma\mu_B\delta h\cdot S_Z \tag{3}$$

with $\delta h=\delta h_0 e^{i\omega t}$ standing for the applied ac magnetic field.

In addition to the term listed in Hamiltonian (2) we also assume the presence of other weak interactions containing terms proportional to $S_+$ or $S_-$, such as spin-orbit interactions or hyperfine interactions, for instance. These terms are responsible for transitions between different spin states. The kinetic equations for the populations $p_m$ of the various total electronic spin states with energy $E_m$ are then written

$$\dot{p}_m=-w_{m+1,m}p_m-w_{m-1,m}p_m+w_{m,m+1}p_{m+1}+w_{m,m-1}p_{m-1} \tag{4}$$

and can be expressed in compact form as

$$\dot{\mathbf{p}}=\underline{W}\mathbf{p}. \tag{5}$$

Here $m$ is the eigenvalue of $S_Z$ and ranges from $-10$ to $+10$ and $\mathbf{p}=(p_{-10},p_{-9},\ldots,p_9,p_{10})$ describes the corresponding occupation probabilities of the states $E_m$. $\underline{W}$ is the transition probability matrix:

$$\underline{W}=\begin{bmatrix} -w_{10,9} & w_{9,10} & \square & \square & \square & 0 & 0 \\ w_{10,9} & -w_{9,8}-w_{9,10} & & & & & 0 \\ \square & & \square & & & & \square \\ \square & & & \square & & & \square \\ \square & & & & \square & & \square \\ 0 & & & & & -w_{-9,-8}-w_{-9,-10} & w_{-9,-10} \\ 0 & 0 & \square & \square & \square & w_{-9,-10} & -w_{-9,-10} \end{bmatrix}. \tag{6}$$

Here $w_{m,n}$ stands for $w_{m\to n}$. Following Lascialfari *et al.*[6] we assume that the magnetization relaxation proceeds with $\Delta m = \pm 1$ transitions due to spin-phonon interactions. Expanding $\mathbf{p}(t)=\mathbf{p}_0+\Delta\mathbf{p}(t)$ where

$$\mathbf{p}_0=\frac{1}{Z}(e^{E_{-10}/kT},e^{-E_{-9}/kT},\ldots,e^{-E_{10}/kT}) \tag{7}$$

and $Z=\Sigma_i \exp(-E_i/kT)$ we obtain

$$\Delta\dot{\mathbf{p}}=\underline{W}(\delta h=0)\cdot\Delta\mathbf{p}+\left(\frac{\partial\underline{W}}{\partial h}\right)_{\delta h=0}\cdot\delta h\cdot\mathbf{p}_0 \tag{8}$$

as

$$\underline{W}\cdot\mathbf{p}_0=0. \tag{9}$$

After some manipulations, we now obtain the frequency-dependent complex susceptibility

$$\chi(\omega)=\frac{g\mu_B\mathbf{S}\Delta\mathbf{p}}{\delta h} \tag{10}$$

as

$$\chi(\omega)=\frac{(g\mu_B)^2}{kT}\cdot\mathbf{S}\cdot\frac{1}{1-i\omega\underline{W}^{-1}}\cdot\underline{S}\cdot\mathbf{p}_0. \tag{11}$$

Here we introduced the vector $\mathbf{S}=\mathbf{m}=(-10,-9,...,9,10)$ and the diagonal matrix $\underline{S}$:

$$\underline{S}=\begin{bmatrix} -S & & & & \\ & -S+1 & & & \\ & & \cdot\cdot & & \\ & & & \cdot\cdot & \\ & & & & S \end{bmatrix} \tag{12}$$

The spin-phonon transition probability $w_{m,m\pm1}$ (Refs. 2 and 6) is magnetic-field dependent and is given by

$$w_{m,m\pm1}=C\frac{(E_{m\pm1}-E_m)^3}{e^{(E_{m\pm1}-E_m)/kT}-1}, \tag{13}$$

where $m$ goes from $-10$ to $+10$. $C$ measures the strength of the spin-phonon coupling and is given by[2,6] $C=(3/2\pi\rho\nu^5\hbar^4)|\langle m|V|m\pm1\rangle|^2$ where $\nu$ is the phonon velocity and $V$ is the operator of the spin-phonon interaction. It should be mentioned that in case of susceptibility measurements, where we study the response to small magnetic fields, the spin-phonon transition probability is in the first approximation magnetic-field independent. This is, however, not true in the presence of a large external magnetic field.

The calculated temperature dependences of the real ($\chi'$) and imaginary ($\chi''$) parts of the calculated ac magnetic susceptibility are shown in Fig. 1 for $\omega$=0, 1, 10, $10^2$, and $10^3$ Hz and different values of the $C$ constant ranging from $C=10^3-10^5$ s$^{-1}$. The corresponding Argand plots $\chi''$ vs $\chi'$ are shown in Fig. 2. In all above cases calculations are made for an activation energy $\Delta=73$ K. The pre-exponential factor $\tau_0$ varied, depending on the value of the electron-phonon coupling constant $C$, between $\tau_0=2.1\times10^{-4}$ s for $C=10^3$ s$^{-1}$ and $\tau_0=2.1\times10^{-6}$ s for $C=10^5$ s$^{-1}$. Below the blocking temperature $\tau$ becomes so large that $\omega\tau\gg1$ and $\chi'(\omega)=C/T$ even for very low frequencies. In this limit the real part of the magnetic susceptibility follows a Curie law whereas the imaginary part $\chi''(\omega)$ drops to zero. It should be, however, mentioned that in this temperature range the spin phonon relaxation mechanism becomes ineffective and the tunneling mechanism takes over.

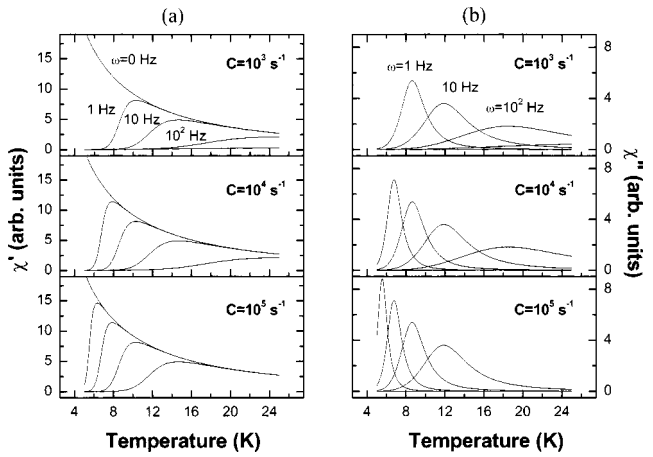


FIG. 1. (a) Computed temperature dependence of the real ($\chi'$) part of the $S=10$ cluster magnetic susceptibility for different frequencies $\omega$ and spin-phonon coupling constants $C$. (b) Computed temperature dependences of the imaginary ($\chi''$) part of the $S=10$ cluster magnetic susceptibility for different frequencies $\omega$ and spin-phonon coupling constants $C$.

### B. NMR spin-lattice relaxation

The NMR spin-lattice relaxation rate is due to hyperfine coupling fluctuations and can serve as a probe for the molecular cluster spin dynamics. It will be evaluated from the same set of kinetic equations in the $S=10$ total spin model as the ac-magnetic susceptibility. The difference is that in view of the presence of the strong magnetic field the magnetization double well potential is now strongly asymmetric. In the

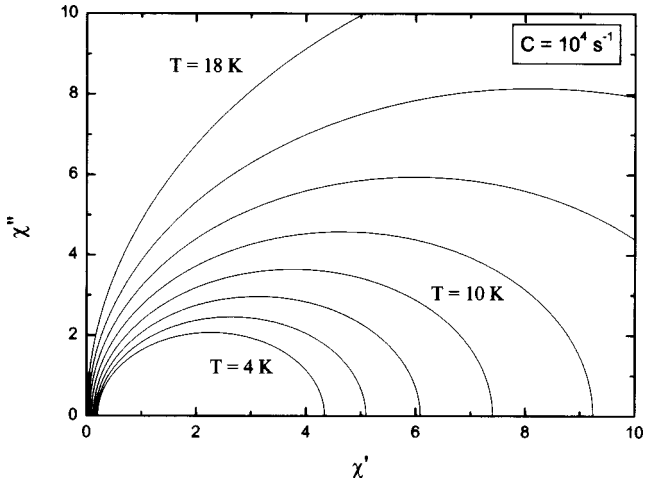


FIG. 2. Argand plots of ($\chi''$) versus ($\chi'$) for the $S=10$ cluster for different temperatures between 4 and 18 K.

applied magnetic field of 9.1 T the second minimum corresponding to the $-m$ states practically disappears.

There are many nonequivalent nuclear sites in the $Mn_{12}$-acetate spin cluster. Let us in the following evaluate the relaxation rate for a given nucleus, e.g., a deuteron, at site *i*. The essential terms of the nuclear spin Hamiltonian are

$$\mathcal{H}=\mathcal{H}_Z+\mathcal{H}_{\rm hpf}, \tag{14}$$

where

$$\mathcal{H}_Z=-\gamma_N\hbar\mathbf{B}\cdot\mathbf{I} \tag{15}$$

stands for the nuclear Zeeman term and

$$\mathcal{H}_{\rm hpf}=\sum_{\alpha,\beta} I_\alpha A_{\alpha\beta} S_\beta, \quad \alpha,\beta=x,y,z \tag{16}$$

for the electron-nuclear hyperfine coupling term. The isotropic part of the hyperfine tensor with components $A_{\alpha\beta}$ is the Fermi contact interaction whereas the anisotropic part describes the electron-nuclear dipolar interactions. The nuclear Hamiltonian can be divided into a time-independent part $\langle\mathcal{H}\rangle$, which determines the NMR spectrum, and a time-dependent part $\mathcal{H}(t)$, which is responsible for the spin-lattice relaxation:

$$\mathcal{H}=\langle\mathcal{H}\rangle+\mathcal{H}(t). \tag{17}$$

The time-dependent part of the Hamiltonian for the molecular cluster in spin state *m* can be expressed as

$$\mathcal{H}^m_{\rm hpf}(t)=\sum_{\alpha,\beta} I_\alpha A_{\alpha\beta} S^{(m)}_\beta(t), \tag{18}$$

where

$$S^{(m)}_\beta(t)=\langle m|S_\beta(t)|m\rangle. \tag{19}$$

The nuclear-spin transition probability $W^{(m)}_{M\to M-1}$ depends on the Fourier transform of the autocorrelation function of the matrix elements of $\mathcal{H}^m_{\rm hpf}(t)$ at the Larmor frequency $\omega_L$:

$$W^{(m)}_{M\to M-1}\propto\int_{-\infty}^{\infty}\overline{\langle M|\mathcal{H}^m_{\rm hpf}(t)|M-1\rangle\langle M-1|\mathcal{H}^{m*}_{\rm hpf}(0)|M\rangle}\cdot e^{-i\omega_L t}dt. \tag{20}$$

The relaxation is produced by the hyperfine field perpendicular to the nuclear axis of quantization.

For the sake of convenience we can introduce the effective hyperfine field at the nuclear site, which is for a given electron spin state *m*,

$$h^m_\alpha(t)=\sum_\beta A_{\alpha\beta}\langle m|S_\beta(t)|m\rangle \tag{21}$$

and

$$h_\pm(t)=h_x(t)\pm ih_y(t). \tag{22}$$

The term $h^{(m)}_Z(t)I_Z$ does not contribute to the nuclear-spin relaxation.

In the case of protons ($I=\frac{1}{2}$) and deuterons ($I=1$), the nuclear magnetization of a single nuclear spin decays monoexponentially (see the Appendix), with a spin-lattice relaxation rate given by

$$\frac{1}{T_1}\propto J(\omega_L)=\int_{-\infty}^{+\infty}\langle h_+(0)h_-(t)\rangle\cdot e^{-i\omega_L t}dt, \tag{23}$$

where

$$\langle h_+(0)h_-(t)\rangle=\frac{1}{Z}\sum_{m=-10}^{+10} e^{-E_m/kT}\overline{h^{(m)}_+(0)h^{(m)}_-(t)}. \tag{24}$$

We now evaluate the autocorrelation function $\langle h_+(0)h_-(t)\rangle$ and the related spectral density $J(\omega_L)$ with the help of the kinetic equations as discussed in the previous chapter. This approach implies that all the hyperfine field autocorrelation function terms containing the cluster spin components $S_x$ and $S_y$ shall be disregarded, i.e., $\langle h_+(0)h_-(t)\rangle\approx(A^2_{xz}+A^2_{yz})\langle S_z(0)S_z(t)\rangle$. We assume that at $t=0$ only the state with $m=m'$ (determined by the strong external magnetic field) is occupied. The fluctuation in the magnetic field then spreads out to all magnetic states until thermal equilibrium is reached. Finally one averages over all initial states so that we get

$$\frac{1}{T_1}=J(\omega_L)=A^2_{\perp z}\overline{\mathbf{m}}'^T(\underline{W}-i\omega_L\underline{1})^{-1}\overline{\mathbf{m}}, \tag{25}$$

where

$$\mathbf{m}=\begin{bmatrix}10\\9\\\cdots\\-9\\-10\end{bmatrix}=\mathbf{S},\quad \mathbf{m}'^T=\frac{1}{Z}\begin{bmatrix}10e^{-E_{10}/hT}\\9e^{-E_9/hT}\\\cdots\cdots\\-9e^{-E_9/hT}\\-10e^{-E_{10}/hT}\end{bmatrix}=\mathbf{p}_0 \tag{26}$$

and $A^2_{\perp z}=A^2_{xz}+A^2_{yz}$. The transition matrix $\underline{W}$ is defined by Eq. (6) and is now strongly magnetic-field dependent. The resulting spectral density-frequency-inverse temperature surface is shown in Fig. 3. The results differ significantly from the ones obtained for a simple exponential decay of the autocorrelation function. Since $(T_1^{-1})$ is different for different nuclear sites *i* we have a relaxation rate distribution $w(T_1^{-1})$ instead of a single $(T_1^{-1})$. The nuclear magnetization recovery will be thus nonexponential as indeed observed in previous $^1$H and D NMR experiments:[6,15]

$$M(t)=M_0\left[1-\int w(T_1^{-1})e^{-t/T_1}d(T_1^{-1})\right]. \tag{27}$$

Expression (27) can be in the present case fitted to a phenomenological stretched exponential decay form:[15]

$$M(t)=M_0[1-e^{-(t/T_1)^\alpha}]. \tag{28}$$

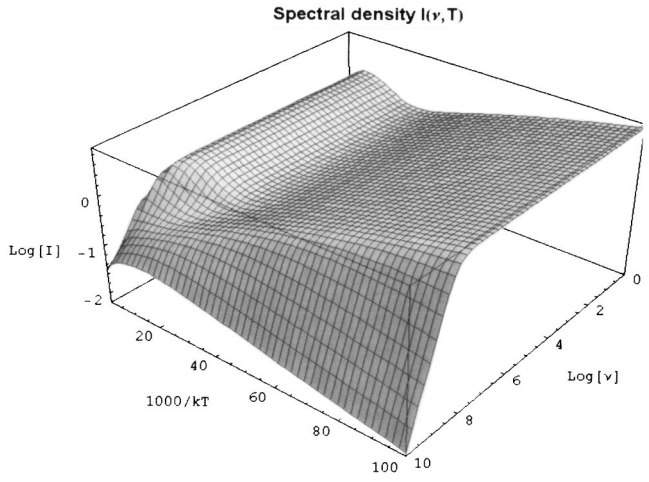


FIG. 3. Computed spectral density-frequency-inverse temperature surface for the deuteron spin-lattice relaxation rate in the $Mn_{12}$-acetate.

## III. EXPERIMENTAL TECHNIQUES AND RESULTS

### A. Magnetic susceptibility

The frequency-dependent complex magnetic susceptibility $\chi^*(\omega,T)=\chi'-i\chi''$ was measured in frequency range from 100 Hz to 1 MHz by a bridge technique using an HP4282 Precision LCR Meter. In a temperature scanning run, the data were taken on cooling or heating the system with a typical rate of $\pm 0.1$ K/min.

The powder samples were ground to fine dust and then pressed (in order to prevent any reorientation) into a specially prepared ceramic cell of volume $2\times 2\times 0.8$ mm$^3$ without using any additives. The temperature- and frequency-independent background value of the empty cell was later subtracted from the susceptibility data.

Figure 4 shows the temperature dependence of the imaginary part of the complex magnetic susceptibility of undeuterated as well as deuterated $Mn_{12}$-acetate systems at different frequencies. Both exhibit a pronounced dispersion in the magnetic susceptibility below 20 K. Peaks in the imaginary part of the complex magnetic susceptibility in the temperature range from 16 to 10 K indicate slowing down of the magnetic relaxation. They occur at different temperatures, indicating an H/D isotope effect in the magnetization dynamics on deuteration. A more comprehensive representation of the magnetic relaxation in an Argand plot [Fig. 5(a)] for undeuterated $Mn_{12}$-acetate indeed confirms the existence of at least one polydispersive magnetic mode below 20 K. The Argand plots were analyzed by the standard Cole-Cole ansatz:

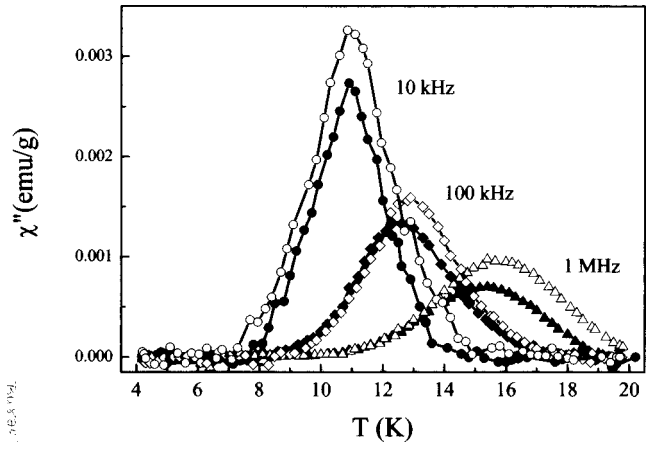


FIG. 4. Temperature dependence of the imaginary part of the magnetic susceptibility of undeuterated and fully deuterated $Mn_{12}$-acetate at different frequencies showing an isotope effect in the magnetization dynamics. Circles represent the measurements at 10 kHz, squares at 100 kHz while triangles stand for 1-MHz measurements. In all cases the solid symbols were used for undeuterated while open symbols were used for deuterated samples.

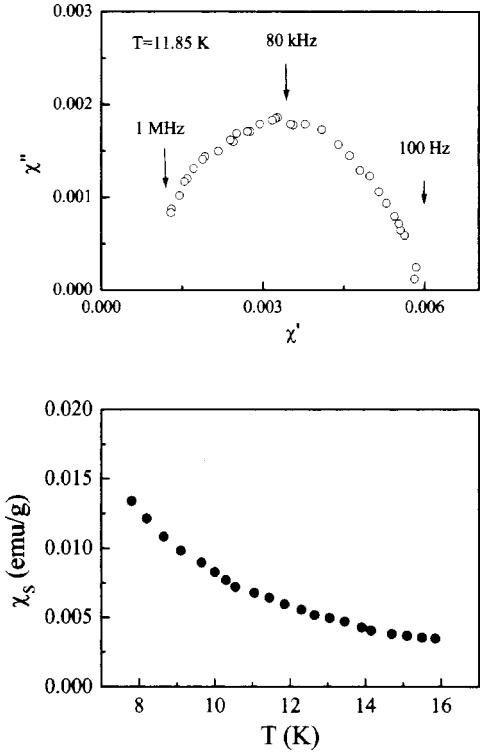


FIG. 5. (a) Argand plot of $\chi''$ vs $\chi'$ for undeuterated $Mn_{12}$-acetate at $T=11.85$ K. (b) The temperature dependence of the static magnetic susceptibility extracted from the Argand plots at different temperatures.

$$\chi^*(\omega,T)=\chi_\infty+\frac{\Delta\chi}{1+(i\omega\tau)^\beta}. \tag{29}$$

Here $\Delta\chi=\chi_S-\chi_\infty$ and $\chi_S$ and $\chi_\infty$ are the static magnetic susceptibility and the high-frequency magnetic background contribution, respectively, whereas $\tau$ is the characteristic relaxation time. The parameter $\beta$ measures the degree of the polydispersivity and was found to be a temperature-independent quantity in both undeuterated and fully deuterated samples, its value ranging around 0.7.

Figure 5(b) shows the temperature dependence of the static magnetic susceptibility $\chi_S$ as extracted from Argand plots for the undeuterated sample. A clear Curie plot is ob-

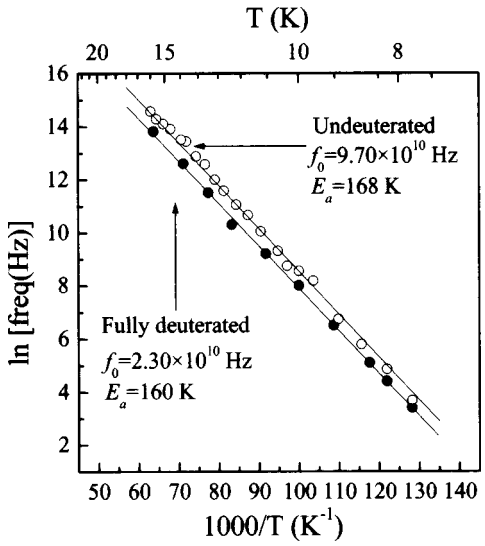


FIG. 6. Temperature dependence of the relaxation frequencies $f=1/2\pi\tau$ of undeuterated and deuterated $Mn_{12}$-acetate.

tained for undeuterated as well as deuterated $Mn_{12}$-acetate. It should be noted that a similar Curie behavior was recently observed by dc magnetic susceptibility measurements.[6] This seems to prove that our data indeed reflect the magnetization reorientation dynamics.

Figure 6 shows the temperature dependence of the relaxation frequencies $f=1/2\pi\tau$ for the undeuterated and fully deuterated sample, respectively, determined by fitting the magnetic susceptibility data to the ansatz (29). The straight lines in Fig. 7 imply a thermally activated Arrhenius-type behavior, $f=f_0\exp(-E_a/k_BT)$, for the relaxation time with the following fitting parameters: $f_0=(9.7\pm2.0)\times10^{10}$ Hz and $E_a/k_B=168\pm5$ K for the undeuterated sample and $f_0=(2.3\pm0.6)\times10^{10}$ Hz and $E_a/k_B=160\pm5$ K for the fully deuterated sample. The observed pre-exponential factors as well as the activation energies and relaxation rates differ considerably from those obtained previously from low-temperature–low-frequency data.[1–6]

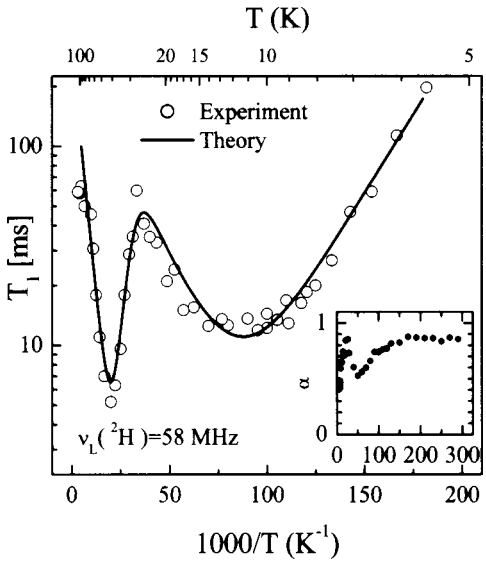


FIG. 7. Temperature dependence of the deuteron spin-lattice relaxation time parameters $T_1$ at $\omega_L/2\pi=58$ MHz extracted from a stretched exponential fit to the nuclear magnetization recovery curves. The temperature dependence of the stretched exponent $\alpha$ is shown in the inset.

It is interesting to note that within the experimental error the activation energy $E_a$ did not change significantly with deuteration while the magnitude of the attempt frequency $f_0$ of the magnetic mode decreased by a factor of 4 in the fully deuterated sample. This demonstrates the existence of a significant isotope effect in the magnetization reversal dynamics on deuteration. A similar isotope effect was found in the case of some of the recently observed dielectric relaxation modes associated with the motion of $H_2O$ and COOH molecules in $Mn_{12}$-acetate[19] and may reflect deuteration induced changes in the H-bond structures. As already mentioned the activation energies for the dielectrically active modes are by at least an order of magnitude higher than the ones for the magnetic modes so that a clear-cut distinction between these two sets of modes is possible.

It should be noted that the above activation energy values are for about 100 K larger than those obtained from low-temperature data.[1–6] However, previously reported results have been obtained in the frequency range below 10 kHz and in the temperature range below 10 K. As reported in Ref. 17, a deviation from Arrhenius behavior was observed at temperatures around 10 K and above, where there is a considerable increase in the activation energy.

It is conceivable that our data, which were performed at higher frequencies (up to 1 MHz) and higher temperatures (up to 20 K), are actually probing the Arrhenius behavior just before it reaches the crossover region, i.e., the Arrhenius behavior with a higher activation energy.

### B. Deuteron spin-lattice relaxation

The temperature dependence of the deuteron spin-lattice relaxation rate was studied with both the inversion recovery and the saturation recovery pulse sequences from the Fourier transform of the echo decay at 9.0 T between 4 and 293 K. The sample was prepared in the same way as for the ac-susceptibility measurements. The deuteron Larmor frequency was 58 MHz. The relaxation rate was measured on the least shifted (i.e., $-CD_3$) deuteron NMR line.[15]

The nuclear magnetization recovery was studied over five decades and was in all cases found to be strongly nonexponential. We note that $^1H$ magnetization recovery curves[6] were also strongly nonexponential and the effective spin-lattice relaxation time was estimated from the initial slope of the magnetization recovery curve. Our data could be fitted either with a stretched exponential form [Eq. (26)] or with a three exponential fit with nearly the same accuracy.

As it can be seen from Fig. 7 the deuteron $T_1$ decreases with decreasing temperature on cooling from room temperature down to about 50 K where a Bloembergen-Purcell-Pound (BPP)-type $T_1$ minimum[20] is reached. Below the minimum $T_1$ increases with decreasing temperature reaching a maximum at around 25 K. After that $T_1$ decreases again with decreasing temperature, reaches a flat $T_1$ minimum be-

tween 10 and 15 K after which it strongly increases with decreasing temperature on approaching the blocking temperature. Our present data at 58 MHz thus roughly agree with the previous ones at 41 MHz.[15] In our previous study we as well used a stretched exponential fit and as well found two deuteron $T_1$ minima as in the present study. The differences can be attributed to the experimental errors involved in the stretched exponential fit and the slight difference in the Larmor frequencies. The high-temperature deuteron $T_1$ minimum occurring between 50 and 70 K correlates well with the minimum observed in the proton $T_1$ around 60 K at Larmor frequencies 87 and 200 MHz.[6] The low-temperature deuteron $T_1$ minimum occurring around 10 K was not seen in the proton $T_1$ measurements probably due to the too short proton $T_1$ values involved. Considering the electronic nuclear energy conservation requirement we should mention that the existence of proton and deuteron $T_1$ minima seems to prove that we are dealing with BPP-type direct spin-lattice relaxation processes[20] rather than with two-phonon Raman processes as involved for Mn $T_1$ data.[13] In this latter case no $T_1$ minimum is expected. An additional support for this fact is given by the strong Larmor frequency dependence of the proton $T_1$ data[6] between 200 and 14 MHz. Such a Larmor frequency dependence cannot be explained by Raman processes. The difference in the rate determining spin-lattice relaxation mechanisms for Mn $T_1$ on one side[13] and $^1$H and $^2$H $T_1$ on the other side may be the rather different Larmor frequencies involved in these two cases. The Mn Larmor frequencies occur between 300 and 500 MHz and thus approach the range where two-phonon processes usually become more effective than direct one-phonon processes.

The minimum around 50 K corresponds to a thermally activated electron-spin correlation time $\tau = \tau_0 \exp(E_a/kT)$ with $E_a \cong 200-250$ K and an attempt frequency $f_0 = 1/2\pi\tau_0 \approx 0.4\times 10^{10}$ Hz. Both the activation energy and the attempt frequency are in our deuterated sample higher than in protonated $Mn_{12}$-acetate and are within the limits of the fitting uncertainty comparable with the ac magnetic susceptibility data ($E_a = 160$ K) described in the previous section. Both activation energies are much higher than the values (66 K) obtained from low-temperature–low-frequency magnetization reversal measurements described in the literature.

An important question is the origin of the two $T_1$ minima. The easiest explanation would be that we have two different relaxation mechanisms characterized by two different correlation times $\tau$ as discussed previously.[15] We believe that this explanation is not realistic in view of the fact that two relaxation rates have not been seen in our dynamic susceptibility measurements. It should be also mentioned that dielectric relaxation data, which are susceptible to $H_2O$ dipole reorientations, gave activation energies exceeding 1000 K, i.e., activation energies which are by a factor of 10 higher than the ones observed in susceptibility measurements and deuteron spin-lattice relaxation data. This means that the two minima involved are indeed related with magnetization reversal processes and not with molecular reorientations.

According to our opinion the two minima reflect the fact that the electronic spin states at the top of the barrier have a very different relaxation rate from the states at the bottom of the potential well. This is indeed reflected in the relaxation rate versus frequency versus temperature surface (Fig. 3) obtained from our model calculations.

Another problem is the origin of the nonexponential nuclear magnetization recovery process, which we described by a stretched exponential fit. We have more than 56 different nuclear hydrogen sites with different relaxation rates in the $Mn_{12}$-acetate spin cluster. It is therefore clear that we have a spin-lattice relaxation rate distribution, which can be simulated by a stretched exponential nuclear magnetization relaxation behavior. The accuracy of the correlation times extracted from the magnetization recovery curves depends on the stretched exponential exponent $\alpha$. The stretched exponent $\alpha$ is of the order of 0.8 from room temperature down to 80 K. It decreases to about 0.6 around 50 K and than exhibits a rather anomalous behavior. It increases to $\alpha \sim 0.85$ at 10 K and then decreases to 0.4 on cooling to 4 K.

Since the shape of the low-temperature $T_1$ minimum is affected by the anomalous temperature dependence of the stretched exponent $\alpha$, we decided to check the reliability of the above data by using a three-exponential fit for the magnetization recovery. At 55 K we then obtain that 29% of the deuteron magnetization relaxes with a $(T_1)_a$ of $\cong 1$ ms, 33% with a $(T_1)_b \cong 6$ ms, and 38% with a $(T_1)_c \cong 81$ ms. All three components are temperature dependent and first decrease and then increase with decreasing temperature. The long $(T_1)_c$ component shows a broad $T_1$ minimum centered around 19 K, the intermediate $(T_1)_b$ exhibits a sharp minimum around 50 K and the short $(T_1)_c$ component a not very pronounced minimum around 30 K. The correlation time values extracted from these minima are within an order of magnitude similar to the ones obtained from the stretched exponential fit. Nevertheless, we believe that in view of the large number of nonequivalent deuteron sites, the stretched exponential fit better reflects the real physical situation than the three exponential fit.

It should be stressed that the deuteron $T_1$ data yield electron-spin-correlation rates $\tau^{-1}$, which are by two orders of magnitude faster than the ones determined from low-temperature–low-frequency susceptibility measurements. This result agrees both with previous proton $T_1$ data[6] as well as with our dynamic susceptibility measurements above the blocking temperature. The deuteron $T_1$ data also confirm the occurrence of an isotope effect in the magnetization dynamics on deuteration.

## IV. CONCLUSIONS

We have presented a model for the electron-spin dynamics in the $Mn_{12}$-acetate spin cluster where not only the ground but also all higher excited electron spin states are taken into account. We used this model for the determination of the ac-magnetic susceptibility and the deuteron NMR spin-lattice relaxation rate in the temperature range where the electron-spin dynamics is determined by phonon assisted jumps of the $Mn_{12}$-acetate cluster magnetization over the potential barrier. The obtained results were compared with magnetic susceptibility and deuteron $T_1$ measurements in the

temperature range above the ''blocking'' temperature. Our results show:

(i) There is a significant isotope effect in the magnetization reversal dynamics of $Mn_{12}$-acetate on deuteration at temperatures $T>10$ K.

(ii) The molecular cluster spin relaxation rates and the activation energy obtained from our high-temperature–high-frequency magnetic susceptibility and deuteron NMR $T_1$ data are significantly higher than the one obtained from the low-frequency–low-temperature magnetization switching and susceptibility data.

The observed isotope effects in the magnetization dynamics reflect the change in the phonon velocity and spin phonon coupling due to change in the strength of the hydrogen bonding of water molecules on deuteration.

Our observations also show that there is a crossover from the low activation energy to a high activation energy behavior and magnetization reversal dynamics around 10 K. This seems to show that at higher temperatures and frequencies the magnetic relaxation of the cluster can no longer be described by the fluctuations of its total spin $S=10$,[13] and that a microscopic approach involving individual $Mn^{3+}$-$Mn^{4+}$ spins is necessary.

## APPENDIX: DEUTERON MAGNETIZATION DECAY FOR RELAXATION VIA HYPERFINE FIELD FLUCTUATIONS

A given deuteron with a spin 1 has three energy levels, 1, 0, $-1$, in an external magnetic field. The population equations for the nuclear spin $I=1$ induced by hyperfine field fluctuations are thus

$$\frac{dN_1}{dt}=-(W_{01}+W_{-11})N_1+W_{10}N_0+W_{1-1}N_{-1},$$

$$\frac{dN_0}{dt}=W_{01}N_1-(W_{-10}+W_{10})N_0+W_{0-1}N_{-1},$$

$$\frac{dN_{-1}}{dt}=W_{-11}N_1+W_{-10}N_0-(W_{1-1}+W_{0-1})N_{-1}. \tag{A1}$$

Here $W_{01}=W_{10}=W_{0-1}=W_{-10}=W$ and $W_{-11}=W_{1-1}=0$. The deuteron magnetization is given by $M\propto -1N_{-1}+0N_0+1N_1=N_1-N_{-1}$. This yields

$$\frac{dM}{dt}=-WM \tag{A2}$$

so that the deuteron magnetization decay at a given nuclear site is monoexponential with

$$\frac{1}{T_1}=W_{10}. \tag{A3}$$


[1] D. Gatteschi, A. Caneschi, L. Pardi, and R. Sessoli, Science **256**, 1054 (1994).

[2] J. Villain, F. Hartman-Bourton, R. Sessoli, and R. Rettori, Europhys. Lett. **27**, 159 (1994).

[3] C. Paulsen, J.-G. Park, B. Barbara, R. Sessoli, and A. Caneschi, J. Magn. Magn. Mater. **140–144**, 379 (1995).

[4] Jonathan R. Friedman, M. P. Sarachik, J. Tejada, and R. Ziolo, Phys. Rev. Lett. **76**, 3830 (1996).

[5] M. Hennion, L. Pardi, I. Mirebeau, E. Suard, R. Sessoli, and A. Caneschi, Phys. Rev. B **56**, 8819 (1997).

[6] A. Lascialfari, Z. H. Jang, F. Borsa, P. Carretta, and D. Gatteschi, Phys. Rev. Lett. **81**, 3773 (1998); see also A. Lascialfari, D. Gatteschi, F. Borsa, A. Shastri, Z. H. Jang, and P. Carreta, Phys. Rev. B **57**, 514 (1998).

[7] J. A. A. J. Perenboom, J. S. Brooks, S. Hill, T. Hathaway, and N. S. Dalal, Phys. Rev. B **58**, 330 (1998).

[8] T. Kubo, T. Koshiba, T. Goto, A. Oyamada, Y. Fujii, K. Takeda, and K. Awaga, Physica B **294–295**, 310 (2001).

[9] T. Goto, T. Kubo, T. Koshiba, Y. Fujii, A. Oyamada, J. Arai, K. Takeda, and K. Awaga, Physica B **284–288**, 1227 (2000).

[10] Z. H. Jang, A. Lascialfari, F. Borsa, and D. Gatteschi, Phys. Rev. Lett. **84**, 2977 (2000).

[11] N. V. Prokofev and P. C. E. Stamp, Phys. Rev. Lett. **80**, 5794 (1998).

[12] S. Hill, J. A. A. J. Perenboom, N. S. Dalal, T. Hathway, T. Stalcup, and J. S. Brooks, Phys. Rev. Lett. **80**, 2453 (1998).

[13] S. Yamamoto and T. Nakanishi, Phys. Rev. Lett. **89**, 157603 (2002).

[14] J. Dolinšek, D. Arčon, R. Blinc, P. Vonlanten, J. L. Gavilano, H. R. Ott, R. M. Achey, and N. S. Dalal, Europhys. Lett. **42**, 691 (1998).

[15] D. Arčon, J. Dolinšek, T. Apih, R. Blinc, N. S. Dalal, and R. M. Achey, Phys. Rev. B **58**, R2941 (1998).

[16] R. M. Achey, P. L. Kuhns, A. P. Reyes, W. G. Moulton, and N. S. Dalal, Phys. Rev. B **64**, 064420 (2001); Solid State Commun. **121**, 107 (2002).

[17] A. M. Gomes, M. A. Novak, R. Sessoli, A. Caneschi, and D. Gatteschi, Phys. Rev. B **57**, 5021 (1998).

[18] P. Langan, R. Robinson, P. J. Brown, D. Argyriou, D. N. Hendrickson, and G. Christou, Acta Crystallogr., Sect. C: Cryst. Struct. Commun. **C57**, 909 (2001).

[19] Z. Kutnjak, C. Filipič, A. Levstik, R. M. Achney, and N. S. Dalal, Phys. Rev. B **59**, 11 147 (1999).

[20] A. Abragam, *Principles of Nuclear Magnetism* (Oxford University Press, Oxford, 1961).